Electronic phase transition from semiconducting to metallic in cubic halide NaGeBr$_3$ perovskite under hydrostatic pressure

Student ID: 181315
Session: 2018-2019

Report submitted to the Department of Physics at
Jashore University of Science and Technology
in partial fulfillment of the requirements
for the degree of Bachelor of Science
with Honours in Physics

January 2024

Abstract

By using density functional theory (DFT) as implemented in WIEN2k, we examine the structural, electronic, optical, and thermoelectric properties of $NaGeBr_3$ perovskite under hydrostatic pressures ranging from 0 to 4 GPa. The structural investigation of the cubic $NaGeBr_3$ perovskite is determined by the Perdew Burke Ernzerhof-Generalized Gradient Approximation (PBE-GGA) functional that reveals the optimized lattice constant is 5.52 Å, which is good agreement with previous study. We calculate electronic, optical and thermoelectric properties by using the Trans Blaha-modified Becke Johnson (TB-mBJ) potential to obtain more accurate energy band gap. Band gap becomes zero from 0.81 eV to 0.00 eV with the increment of pressure from 0 GPa to 4 GPa, enhancing it's conductivity. The optical response of $NaGeBr_3$ are inspected by computing absorption coefficient, complex dielectric function, refractive index, reflectivity, extinction coefficient, electron energy loss, and optical conductivity. Thermoelectric properties of $NaGeBr_3$ are investigated in terms of electrical conductivity, the Seebeck coefficient, power factor, thermal conductivity by using the BoltzTraP code. $NaGeBr_3$ is found to be have good potential to be used in developing lead-free perovskite solar cells and other optoelectronic applications.

Acknowledgements

Contents

Contents

List of Figures

List of Tables

Electronic phase transition from semiconducting to metallic in cubic halide NaGeBr$_3$ perovskite under hydrostatic pressure

Chapter 1

Introduction

Over the decades, the use of photovoltaic (PV) and optoelectronic devices has increased significantly [1–3]. Scientists are still looking for materials that will be highly efficient for solar cells and other optoelectronic devices, which are environment friendly and affordable. In this concern, numerous investigations on cubic halide perovskite compounds have been carried out. They have all the potential to develop into innovative materials such as semiconductor [4, 5], half metal [6–8] and insulator [9, 10]. The halide perovskites are utilized in different fields of remarkable applications like sensors [11], solar cells [12–14], superconductivity [15], piezoelectricity [16, 17], diodes and transparent coatings [18, 19]. Most of these devices are manufactured on a large scale for solar to fuel energy conversion [20–23].

Perovskites was originally discovered in 1939 by Gustav Rose, a Russian mineralogist in a chunk of chlorite-rich skarn [24]. The general formula of the cubic perovskite is ABX_3, where A and B represent the cations and X (oxygen or halogen) is the anion [25, 26]. Most of the halide perovskites with excellent properties comprise of lead (Pb) which is toxic and harmful for the environment [27–29]. As an alternative, lead-free halide perovskites are capable of attracting the attention of scientists [30–33], because of their nature friendly non-toxic features. Thus, perovskites based on Ge have emerged as a possible alternative of lead (Pb), because they possess superior

1

optical absorptivity and conductivity as compared to Pb-based perovskites [34]. An overview of the computational analysis on the structural and electrical characteristics of $CsMgBr_3$ for all three phases was presented by Kaewmeechai et al. [35]. Mohammad Abdur Rashid et al. investigated the metallic behavior of semiconducting lead-free halide perovskites $RbSnX_3$ (X , Cl, Br) under pressure. They observed that the optical absorbance and conductivity of the perovskites are appropriate for optoelectronic applications [30]. Recent studies have demonstrated that inorganic halide perovskites, including $AGeF_3$ (A = K, Rb), $KGeX_3$ (X = Cl, Br, I), $CsGeX_3$ (X = Cl, Br) exhibit a decrease in band gap under hydrostatic pressure, leading to an enhancement in conductivity. Furthermore, pressure application can significantly improve the optical characteristics of halide perovskites, improving their utility in optoelectronic areas [36–42].

Therefore, we are motivated by the above work to investigate the structural, electronic, optical, and thermoelectric properties of the perovskite material $NaGeBr_3$ at ambient and hydrostatic pressure to provide information on its potential applications in solar cells and other optoelectronic devices. The work is structured as follows: an introduction is given in Chapter 1, and theoretical background is covered in Chapter 2. Further, we have elaborately discussed the results in Chapter 3 and the conclusion of the current study in Chapter 4.

<div align="right">

Chapter 2

</div>

Theoretical background

2.1 Schrödinger equation

The Schrödinger equation is a second order linear partial differential equation of quantum mechanics for the study of microscopic events. In 1926, The Schrödinger equation, developed by the Austrian scientist Erwin Schrödinger [43]. The energy operator, or Hamiltonian, is crucial in quantum mechanics because it uses the Schrödinger equation to describe how the system change [44]. The time-independent Schrödinger equation is the energy eigenvalue of the hamiltonian multiplied by the wave function, leading the general eigenvalue equation as

$$\hat{H}\psi(\mathbf{r}) = \hat{E}\psi(\mathbf{r}), \tag{2.1}$$

where $\hat{H}$ is the Hamiltonian operator, $\hat{E}$ is the energy and ψ is the wave function. Using the Hamiltonian for a single particle

$$\hat{H} = \hat{T} + \hat{V} = -\frac{\hbar^2}{2m}\vec{\nabla}^2 + V(\mathbf{r}), \tag{2.2}$$

that results in the time-independent single-particle Schrödinger equation (non-relativistic)

$$i\hbar\frac{\partial}{\partial r}\psi(\mathbf{r}) = \left[-\frac{\hbar^2}{2m}\vec{\nabla}^2 + V(\mathbf{r})\right]\psi(\mathbf{r}). \tag{2.3}$$

The Hamiltonian in three-dimensions for N-particles

$$\hat{H} = \sum_{i=1}^{N}\frac{{p_i}^2}{2m_i} + V(\mathbf{r}_1, \mathbf{r}_2, ...\mathbf{r}_N). \tag{2.4}$$

The related Schrödinger equation is as follows:

$$i\hbar\frac{\partial}{\partial r}\psi(\mathbf{r}_1, \mathbf{r}_2, ...\mathbf{r}_N) = \left[\sum_{i=1}^{N}\frac{{p_i}^2}{2m_i} + V(\mathbf{r}_1, \mathbf{r}_2, ...\mathbf{r}_N)\right]\psi(\mathbf{r}_1, \mathbf{r}_2, ...\mathbf{r}_N). \tag{2.5}$$

2.2 The wave function

A wave function is a mathematical representation of a particle's quantum state as a function of momentum, position, time and spin in quantum physics. It contains all the information about the particle's state. A wave function is represented by the Greek letter ψ (psi). The probability of finding an electron within the matter-wave may be explained using a wave function. This may be produced by incorporating an imaginary number that is squared to give a real number solution resulting in an electrons position.

Max Born developed a probabilistic interpretation of the wave function as a probability density, which is a major principle of the Copenhagen interpretation of quantum mechanics [45].

$$|\psi(\mathbf{r}_1, \mathbf{r}_2, ...\mathbf{r}_N)|^2 d\mathbf{r}_1, d\mathbf{r}_2, ...\mathbf{r}_N. \tag{2.6}$$

The particles $1, 2, ..., N$ are all present at the same time in the corresponding volume element $d\mathbf{r}_1, d\mathbf{r}_2, ...d\mathbf{r}_N$ which is the probability that is specified by equation (2.6). If the positions of two particles are exchanged, the total probability density cannot be affected. That is to written as,

$$|\psi(\mathbf{r}_1, \mathbf{r}_2, ...\mathbf{r}_i, \mathbf{r}_j, ...\mathbf{r}_N)|^2 = |\psi(\mathbf{r}_1, \mathbf{r}_2, ...\mathbf{r}_j, \mathbf{r}_i, ...\mathbf{r}_N)|^2. \tag{2.7}$$

The symmetrical and anti-symmetrical wave functions are two possible wavefunction behaviours during a particle exchange. The symmetrical wave function remains unchanged as a result of such exchange, which corresponds to bosons (integer or zero spin). However, the anti-symmetrical wave function shifts it's sign to correspond to fermions (half-integer spin) [46]. Because electrons are fermions, in this text may explore the anti-symmetric fermion wave function. The Pauli exclusion principle, which states that no two electrons may occupy the same orbital, is followed by the anti-symmetric fermion wave function. Another result of probability interpretation is the normalization of the wave function [47]. A particle's wave function must be normalized. The probability of finding the particle somewhere in space is unity as

$$\int d\mathbf{r}_1 \int d\mathbf{r}_2 ... \int d\mathbf{r}_N |\psi(\mathbf{r}_1, \mathbf{r}_2, ...\mathbf{r}_N)|^2 = 1. \tag{2.8}$$

Eq.(2.8) is physically valid. Continuous and square-integrable wave functions are required. In quantum physics, any wave function that is not continuous and square-integrable has no physical meaning [48]. When we calculate the expectation values of operators with a wave function, we get the expectation value of the corresponding observable for that wavefunction, which is another important aspect of the wave function. This may be expressed for an observable $O(\mathbf{r}_1, \mathbf{r}_2, ...\mathbf{r}_N)$ as

$$O = \langle O \rangle = \int d\mathbf{r}_1 \int d\mathbf{r}_2 \int d\mathbf{r}_N \psi^*(\mathbf{r}_1, \mathbf{r}_2, ...\mathbf{r}_N)\hat{O}\psi(\mathbf{r}_1, \mathbf{r}_2, ...\mathbf{r}_N). \tag{2.9}$$

2.3   Born-Oppenheimer (BO) approximation

The Schrödinger equation of a many-body system is

$$H_{tot}\psi(\{\mathbf{R}_I\}, \{\mathbf{r}_i\}) = E\psi(\{\mathbf{R}_I\}, \{\mathbf{r}_i\}). \tag{2.10}$$

Where, H_{tot} is the total Hamiltonian, E is the total energy and $\psi(\{\mathbf{R}_I\}, \{\mathbf{r}_i\})$ is the total wave function of the system. The total Hamiltonian of a many-body system

consisting of nuclei and electrons can be written as

$$\hat{H}_{tot} = -\sum_I \frac{\hbar^2}{2M_I} \vec{\nabla}^2_{\mathbf{R}_I} - \sum_i \frac{\hbar^2}{2m_e} \vec{\nabla}^2_{\mathbf{r}_i} + \frac{1}{2} \sum_{I,J} \frac{Z_I Z_J e^2}{|\mathbf{R}_I - \mathbf{R}_J|}$$
$$+ \frac{1}{2} \sum_{i,j} \frac{e^2}{|\mathbf{r}_i - \mathbf{r}_j|} - \sum_{I,i} \frac{Z_I e^2}{|\mathbf{R}_I - \mathbf{r}_i|}, \qquad (2.11)$$

where, the indexes I,J run on nuclei, i and j on electrons, $\mathbf{R}_I$ and M_I are position and mass of the nuclei, $\mathbf{r}_i$ and m_e are position and mass of the electrons, $|\mathbf{R}_I - \mathbf{R}_J|$, $|\mathbf{R}_I - \mathbf{r}_i|$ and $|\mathbf{r}_i - \mathbf{r}_j|$ are represent the distance between the nucleus-nucleus, nucleus-electron, and electron-electron.

As nuclei are significantly heavier than electrons (the mass of a proton is about 1836 times the mass of an electron), the electrons travel considerably more quickly than the nuclei [49]. In that case, Born-Oppenheimer (BO) approximation was proposed by Born and Oppenheimer in 1927. The Born-Oppenheimer approximation is an assumption that it is possible to distinguish eq.(2.11) between the nuclear and electronic motions of molecules. After applying Born-Oppenheimer approximation, the Schrödinger equation of many body system is reduced as,

$$\hat{H}_{BO} = -\sum_i \frac{\hbar^2}{2m_e} \vec{\nabla}^2_{\mathbf{r}_i} + \frac{1}{2} \sum_{i,j} \frac{e^2}{|\mathbf{r}_i - \mathbf{r}_j|} - \sum_{I,i} \frac{Z_I e^2}{|\mathbf{R}_I - \mathbf{r}_i|}. \qquad (2.12)$$

The BO approximation's importance lies in it's ability to distinguish between the motion of electrons and nuclei. The starting point of DFT is the electron motion in a static external potential $V_{ext}(\mathbf{r})$ created by the nucleus. Born and Huang expanded the BO approximation, giving it the name Born-Huang (BH) approximation [50], to account for more non-adiabatic effects in the electronic Hamiltonian than the BO approximation did.

2.4 The Hartree-Fock (HF) approach

In the spirit of the Born-Oppenheimer approximation, The electronic equation for molecules that depends parametrically on the nuclear co-ordinates is approximated

using the Hartree-Fock method [45]. Hartree-Fock method is a method of approximation for the determination of the wave function and the energy of a quantum many-body system in a Schrödinger equation. Suppose that, ψ is approximated as an antisymmetrized product of N orthonormal spin orbitals $\psi_i(\mathbf{x})$, each a product of a spatial orbital $\phi_k(\mathbf{r})$ and a spin function $\sigma(s) = \alpha(s)$ or $\beta(s)$, the Slater determinant,

$$\phi_{HF} = \frac{1}{\sqrt{N!}} \begin{vmatrix} \psi_1(\mathbf{x}_1) & \psi_2(\mathbf{x}_1) & \cdots & \psi_N(\mathbf{x}_1) \\ \psi_1(\mathbf{x}_2) & \psi_2(\mathbf{x}_2) & \cdots & \psi_N(\mathbf{x}_2) \\ \vdots & \vdots & \ddots & \vdots \\ \psi_1(\mathbf{x}_N) & \psi_2(\mathbf{x}_N) & \cdots & \psi_N(\mathbf{x}_N) \end{vmatrix}. \tag{2.13}$$

$$= \frac{1}{\sqrt{N!}} det[\psi_1 \psi_2 \cdots \psi_N] \tag{2.14}$$

A general expression for the Hartree-Fock energy is obtained by uses of the Slater determinant.

$$\langle \psi_{HF} | \hat{H} | \psi_{HF} \rangle = E_{HF} \tag{2.15}$$

$$(\sum_{i=1}^{N} H_i + \frac{1}{2} \sum_{i,j}^{N} J_{ij} - K_{ij}) \psi_{HF} = E_{HF} \psi_{HF}. \tag{2.16}$$

Where, the first term corresponds to the kinetic energy and the nucleus-electron interactions. So, the single particle contribution of the Hamiltonian is written as,

$$\hat{H}_i = \int \psi^*(\mathbf{x})[-\frac{1}{2}\nabla^2 + V(\mathbf{x})]\psi_i(\mathbf{x})d\mathbf{x}. \tag{2.17}$$

And the last term of eq.(2.16) correspond to electron-electron interactions. They are called Coulomb (J_{ij}) and exchange integral (K_{ij}). We can write this term in the following way,

$$\hat{J}_{ij} = \int \int \psi_i(\mathbf{x}_1)\psi_j^*(\mathbf{x}_1)\frac{1}{r_{12}}\psi_j^*(\mathbf{x}_2)\psi_j(\mathbf{x}_2)d\mathbf{x}_1 d\mathbf{x}_2. \tag{2.18}$$

$$\hat{K}_{ij} = \int \int \psi_i^*(\mathbf{x}_1)\psi_j(\mathbf{x}_1)\frac{1}{r_{12}}\psi_j(\mathbf{x}_2)\psi_j^*(\mathbf{x}_2)d\mathbf{x}_1 d\mathbf{x}_2. \tag{2.19}$$

These integrals are all real, and $\hat{J}_{ij} \geq \hat{K}_{ij} \geq 0$.

2.4.1 Limitation and failings of the Hartree-Fock (HF) approach

Molecules and atoms can both have an even or an odd number of electrons. The compound is in a single state if the number of electrons is even and they are all positioned in double-occupied spatial orbitals ψ_i. They are reffered to as closed-shell systems. Both substances with one occupied orbital, or species with a triplet or higher ground state, and substances with an odd number of electrons are referred to be open-shell systems. These two types of systems relate to two distinct Hartree-Fock approach. All electrons are assumed to be coupled in orbitals when using the restricted HF approach (RHF), however this restriction is completely eliminated when using the unrestricted HF method (UHF). RHFs may also be used to define open-shell systems [51]. The size of the investigated system can also be a limiting factor for calculations. Kohn states a number of $M = p^5$ with $3p10$ parameters for a result with sufficient accuracy in the investigation of the H_2 system [52]. For a system with $N = 100$ (active) electrons the number of parameters rises to

$$M = p^{3N} = 3^{300} to 10^{300} \approx 10^{150} to 10^{300}. \tag{2.20}$$

Since a many electron wave function cannot be described entirely by a single Slater determinant, the energy obtained by HF calculations is always larger than the exact ground state energy. The most accurate energy obtainable by HF-methods is called the Hartree-Fock-limit. The difference between E_{HF} and E_{exact} is called correlation

energy and can be denoted as [53]

$$E_{corr}^{HF} = E_{min} - E_{HF}. \tag{2.21}$$

Despite the fact that E_{corr} is usually small against E_{min}, as in the example of a N_2 molecule where

$$E_{corr}^{HF} = 14.9eV < 0.001.E_{min}, \tag{2.22}$$

it can have a huge influence [54]. For instance, the experimental dissociation energy of the N_2 molecule is

$$E_{diss} = 9.9eV < E_{corr}, \tag{2.23}$$

which corresponds to a large contribution of the correlation energy to relative energies such as reaction energies which are of particular interest in quantum chemistry. The main contribution to the correlation energy arises from the mean field approximation used in the HF-method. That means one electron moves in the average field of the other ones, an approach which completely neglects the intrinsic correlation of the electron movements. To get a better understanding what that means, one may picture the repulsion of electrons at small distances which clearly cannot be covered by a mean-field approach like the Hartree-Fock method.

2.5   The electron density

The electron density (for N electrons) as the basic variable of density fuctional theory is defined as [55]

$$n(\mathbf{r}) = N \sum_{s_1} \int d\mathbf{x}_2 ... \int d\mathbf{x}_N \psi^*(\mathbf{x}_1, \mathbf{x}_2, ...\mathbf{x}_N)\psi(\mathbf{x}_1, \mathbf{x}_2, ..., \mathbf{x}_N). \tag{2.24}$$

The electron density can also be described as a measurably obserable quantity based simply on spatial coordinates if the spin coordinates are further neglected [56]

$$n(\mathbf{r}) = N \int d\mathbf{r}_2 ... \int d\mathbf{r}_N \psi^*(\mathbf{r}_1, \mathbf{r}_2, ..., \mathbf{r}_N)\psi(\mathbf{r}_1, \mathbf{r}_2, ..., \mathbf{r}_N) \tag{2.25}$$

with, for instance, an X-ray diffraction measurement.

It must be confirmed that a method employing the electron density as a variable actually contains all necessary information about the system before it is presented. That entails, specifically, that it must include details on the electron number n as well as the external potential denoted by $\hat{V}$. By integrating the electron density over the spatial variables, one may get the total number of electrons.

$$N = \int d\mathbf{r}n(\mathbf{r}). \tag{2.26}$$

2.6 Thomas-Fermi-Dirac approximation

In 1927, the predecessor to DFT was the Thomas-Fermi (TF) model proposed by Thomas [57] and Fermi [58]. They used the electron density $n(\mathbf{r})$ as the basic variable instead of the wavefunction. The total energy of a system in an external potential $V_{ext}(\mathbf{r})$ is written as a functional of the electron density $V_{ext}(\mathbf{r})$ as:

$$E_{TF}[n(\mathbf{r})] = A_1 \int n(\mathbf{r})^{\frac{5}{3}} d\mathbf{r} + \int n(\mathbf{r}) V_{ext}(\mathbf{r}) d\mathbf{r} + \frac{1}{2} \int \int \frac{n(\mathbf{r})n(\mathbf{r})'}{|\mathbf{r} - \mathbf{r}'|} d\mathbf{r} d\mathbf{r}'. \tag{2.27}$$

Where the first term is the kinetic energy of the non-interacting electrons in homogeneous electron gas (HEG) with $A_1 = \frac{3}{10}(3\pi^2)^{\frac{2}{3}}$ in the free electron energy state $\epsilon_k = \frac{k^2}{2}$ up to the Fermi wave vector $k_F = [3\pi^2 n(\mathbf{r})]^{\frac{1}{3}}$ as:

$$t_0[n(\mathbf{r})] = \frac{2}{(2\pi)^3} \int_0^{k_F} \frac{k^2}{2} 4\pi k^2 dk$$
$$= A_l n(\mathbf{r})^{\frac{5}{3}}$$

The classical electrostatic energy of the Coulomb interaction between the nucleus and electron is the second term. The classical Coulomb repulsion between electrons, which approximates the classical electrostatic Hartree energy, is the third term. The exchange and correlation between electrons were neglected in the original TF approach. In 1930, Dirac [59] extended the Thomas-Fermi method by adding a local exchange term $A_2 \int n(\mathbf{r})^{\frac{4}{3}} d\mathbf{r}$ to eq.(2.27) with $A_2 = -\frac{3}{4}(\frac{3}{\pi})^{\frac{1}{3}}$, which leads eq.(2.27)

to

$$E_{TFD}[n(\mathbf{r})] = A_1 \int n(\mathbf{r})^{\frac{5}{3}} d\mathbf{r} + \int n(\mathbf{r}) V_{ext}(\mathbf{r}) d\mathbf{r}$$
$$+ \frac{1}{2} \int \int \frac{n(\mathbf{r}) n(\mathbf{r})'}{|\mathbf{r} - \mathbf{r}'|} d\mathbf{r} d\mathbf{r}' + A_2 \int n(\mathbf{r})^{\frac{4}{3}} d\mathbf{r}. \tag{2.28}$$

When the total number of electrons (N) is conserved, The Thomas-Fermi-Dirac eq.(2.28) can be minimized to get the ground state density and energy. In the stationary condition, the solution can be found by applying the Lagrange multiplier method.

$$\delta \{ E_{TFD}[n(\mathbf{r})] - \mu (\int n(\mathbf{r}) d\mathbf{r} - N) \} = 0, \tag{2.29}$$

where μ is a constant known as a lagrange multipliers, whose physical meaning is the chemical potential (or Fermi energy at T $= 0$ K). Eq.(2.29) leads to the Thomas-Fermi-Dirac equation,

$$\frac{5}{4} A_1 n(\mathbf{r})^{\frac{2}{3}} + V_{ext}(\mathbf{r}) + \int \frac{n(\mathbf{r}')}{|\mathbf{r} - \mathbf{r}'|} d\mathbf{r}' + \frac{4}{3} A_2 n(\mathbf{r})^{\frac{1}{3}} - \mu = 0 \tag{2.30}$$

which can be solved directly to obtain the ground state density.

2.7 The Hohenberg-Kohn (HK) theorems

Density functional theory (DFT) is the most widely used many-body approach for electronic structure calculations and has significantly impacted on modern science and engineering. DFT is made possible by the existance of two ingeniously simple theorems put forward and proven by Hohenberg and Kohn in 1964 [60]. The Hohenberg-Kohn theorems which have become a basic tool for the study of electronic structure of matter. Basically, any system that involves electron.

2.7.1 The HK theorem I

For any system of interacting particles in an external potential $V_{ext}(\mathbf{r})$, the density is uniquely determined (in other words, the external potential is a unique functional of the density).

Proof of the HK theorem I

Assume that there exist two potentials $V_{ext}(\mathbf{r})$ and $V'_{ext}(\mathbf{r})$ differing by more than a constant and giving rise to the same ground state density, $n_0(\mathbf{r})$. Obviously, $V_{ext}(\mathbf{r})$ and $V'_{ext}(\mathbf{r})$ belong to distinct Hamiltonians $\hat{H}$ and $\hat{H}'$, which give rise to distinct wavefunctions ψ and ψ'. Because of the variational principle, no wave function can give an energy that is less than the energy of ψ for $\hat{H}$. That is

$$
\begin{aligned}
E_0 &< \langle \psi'|\hat{H}|\psi'\rangle \\
&< \langle \psi'|\hat{H}'|\psi'\rangle + \langle \psi'|\hat{H} - \hat{H}'|\psi'\rangle \\
&< E'_0 + \int n_0(\mathbf{r})[V_{ext}(\mathbf{r}) - V'_{ext}(\mathbf{r})]d\mathbf{r}
\end{aligned}
\tag{2.31}
$$

Similarly

$$
\begin{aligned}
E'_0 &< \langle \psi|\hat{H}|\psi\rangle \\
&< \langle \psi|\hat{H}|\psi\rangle + \langle \psi|\hat{H}' - \hat{H}|\psi\rangle \\
&< E_0 + \int n_0(\mathbf{r})[V'_{ext}(\mathbf{r}) - V_{ext}(\mathbf{r})]d\mathbf{r}.
\end{aligned}
\tag{2.32}
$$

Adding eq.(2.31) and eq.(2.32) lead to the contradiction

$$
E_0 + E'_0 < E_0 + E'_0
\tag{2.33}
$$

which is clearly a contradiction. Thus, the theorem has been proven by reduction absurdum.

2.7.2   The HK theorem II

A universal functional $F[n(\mathbf{r})]$ for the energy $E[\psi']$ can be defined in terms of the density, The exact ground state is the global minimum value of this functional.

Proof of the HK theorem II

Since the external potential is uniquely determined by the density and since the potential in turn uniquely (except in degenerate situations) determines the ground state wavefunction, all the other observables of the system such as kinetic energy are

uniquely determined. Then one may write the energy as a functional of the density. The universal functional $F[n(\mathbf{r})]$ can be written as

$$F[n(\mathbf{r})] \equiv T[n(\mathbf{r})] + E_{int}[n(\mathbf{r})] \qquad (2.34)$$

where $T[n(\mathbf{r})]$ is the kinetic energy and $E_{int}[n(\mathbf{r})]$ is the interaction energy of the particles. According to variational principle, for any wavefunction ψ', the energy functional $E[\psi']$:

$$E[\psi'] \equiv \langle \psi' | \hat{T} + \hat{V}_{int} + \hat{V}_{ext} | \psi' \rangle \qquad (2.35)$$

has its global minimum value only when ψ' is the ground state wavefunction ψ_0 with the constraint that the total number of the particle is conserved. According to HK theorem I, ψ' must correspond to a ground state with particle density $n'(\mathbf{r})$ and external potential $V'_{ext}(\mathbf{r})$, then $E[\psi']$ is a functional of $n'(\mathbf{r})$. According to variational principle:

$$
\begin{aligned}
E[\psi'] &\equiv \langle \psi' | \hat{T} + \hat{V}_{int} + \hat{V}_{ext} | \psi' \rangle \\
&= E[n'(\mathbf{r})] \\
&= \int n'(\mathbf{r}) V'_{ext}(\mathbf{r}) d\mathbf{r} + F[n'(\mathbf{r})] \\
&> E[\psi_0] \\
&= \int n_0(\mathbf{r}) V_{ext}(\mathbf{r}) d\mathbf{r} + F[n_0(\mathbf{r})] \\
&= E[n_0(\mathbf{r})]
\end{aligned}
\qquad (2.36)
$$

Thus the energy functional $E[\psi'] \equiv \int n(\mathbf{r}) V_{ext}(\mathbf{r}) d\mathbf{r} + F[n(\mathbf{r})]$ evaluated for the correct ground state density $n_0(\mathbf{r})$ is indeed lower than the value of this functional for any other density $n(\mathbf{r})$. Therefore by minimizing the total energy functional of the system with respect to variations in the density $n(\mathbf{r})$, one would find the exact ground state density and energy [61]. This functional only determines ground state properties, it doesn't provide any guidance concerning excited states.

2.8 The Kohn-Sham (KS) equations

An inventive indirect method of monoelectronic equation for the kinetic-energy functional $T[n(\mathbf{r})]$ was developed by Kohn and Sham in 1965 as Kohn-Sham (KS) method [62]. Kohn and Sham proposed introducing orbitals into the problem in such a way that the kinetic energy can be computed simply to good accuracy, leaving a small residual correction that is handled separately. It is convenient to begin with the exact formula for the ground-state kinetic energy,

$$T = \sum_i^N a_i \langle \psi_i | - \frac{1}{2}\nabla^2 |\psi_i\rangle \tag{2.37}$$

where, ψ_i and a_i respectively, natural spin orbitals and their occupation numbers. We are assured from the Hohenberg-Kohn theory that this T is a functional of the total electron density.

$$n(\mathbf{r}) = \sum_i^N a_i |\psi_i(\mathbf{r})|^2 \tag{2.38}$$

Kohn and Sham showed that one can built a theory using simpler formulas, namely,

$$T_s[n] = \sum_i^N \langle \psi_i | - \frac{1}{2}\nabla^2 |\psi_i\rangle \tag{2.39}$$

and

$$n(\mathbf{r}) = \sum_i^N |\psi_i(\mathbf{r})|^2 \tag{2.40}$$

This representation of kinetic energy and density holds true for the determinantal wave function that exactly describes N non-interacting electrons. In analogy with the Hohenberg-Kohn defination of the universal functional $F_{HK}[n]$, Kohn and Sham invoked a corresponding non-interacting reference system, with the Hamiltonian,

$$\hat{H}_s = \sum_i^N (\frac{1}{2}\nabla_i^2) + \sum_i^N \nu_s(\mathbf{r}) \tag{2.41}$$

in which there are no electron-electron repulsion terms and for which the ground state electron energy is exactly n. For this system, there will be an exact determi-

nantal ground-state wave function,

$$\psi_s = \frac{1}{\sqrt{N!}} det[\psi_1 \psi_2 \ldots \psi_N] \qquad (2.42)$$

where ψ_i are the N lowest eigenstates of the one-electron Hamiltonian $\hat{h}_s$:

$$\hat{h}_s \psi_i = [-\frac{1}{2}\nabla^2 + \nu_s(\mathbf{r})]\psi_i = \varepsilon_{me}\psi_i \qquad (2.43)$$

The kinetic energy is $T_s(n)$ given by eq.(2.39).

$$T_s[n] = \langle \psi_s | \sum_i^N (-\frac{1}{2}\nabla_i^2)|\psi_i\rangle = \sum_{i=1}^N \langle \psi_i | -\frac{1}{2}\nabla^2|\psi_i\rangle \qquad (2.44)$$

The quantity $T_s[n]$, although uniquely defined for any density, is still not the exact kinetic energy functional. Kohn-Sham set up a problem of interest in such a way that $T_s[n]$ is it's kinetic energy component. To produce the desired separation out of $T_s[n]$ as the kinetic energy component, we write the equation as

$$F[n] = T_s[n] + J[n] + E_{xc}[n]. \qquad (2.45)$$

Where

$$E_{xc}[n] = T[n] - T_s[n] + V_{ee}[n] - J[n] \qquad (2.46)$$

Here the quantity $E_{xc}[n]$ is called exchange-correlation energy. It contains the difference between T and T_s and non-classical part of $V_{ee}[n]$. The Euler equation becomes

$$\mu = \nu_{eff}(\mathbf{r}) + \frac{\delta T_s[n]}{\delta n(\mathbf{r})} \qquad (2.47)$$

Where KS effective potential is defined by

$$\begin{aligned} \nu_{eff}(\mathbf{r}) &= \nu(\mathbf{r}) + \frac{\delta J[n]}{\delta n(\mathbf{r})} + \frac{\delta Exc[n]}{\delta n(\mathbf{r})} \\ &= \nu(\mathbf{r}) + \int \frac{n(\mathbf{r}')}{|\mathbf{r}-\mathbf{r}'|}dr' + \nu_{xc}(\mathbf{r}) \end{aligned} \qquad (2.48)$$

with the exchange-correlation potential

$$\nu_{xc}(\mathbf{r}) = \frac{\delta E_{xc}[n]}{\delta n(\mathbf{r})} \tag{2.49}$$
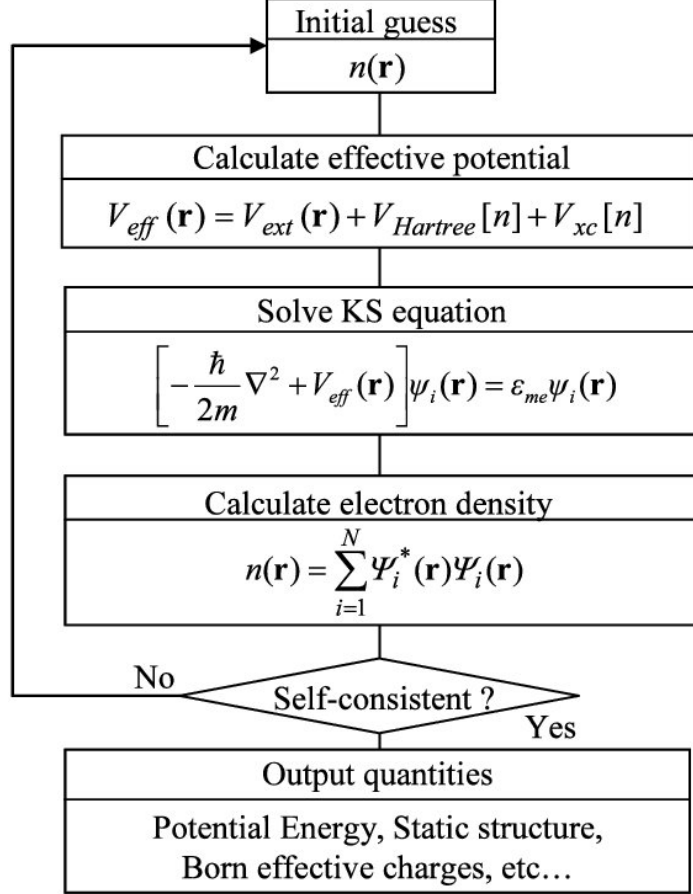
Figure 2.1: Flowchart of self-consistency loop for solving Kohn-Sham equations

For a system of non-interacting electrons moving in the external potential $\nu_s(\mathbf{r}) = \nu_{eff}(\mathbf{r})$. Therefore, for a given $\nu_{eff}(\mathbf{r})$, one obtains the $n(\mathbf{r})$ that satisfies eq.(2.49) simply by solving the N-one electron equations,

$$[-\frac{1}{2}\nabla^2 + \nu_{eff}(\mathbf{r})]\psi_i = \varepsilon_{me}\psi_i \tag{2.50}$$

where ε_{me} is the eigenvalue of monoelectron equation and setting

$$n(\mathbf{r}) = \sum_i^N |\psi_i(\mathbf{r})|^2 \tag{2.51}$$

Eq.(2.48) and eq.(2.51) are celebrated Kohn-Sham equations.

The Kohn-Sham equations derived above that are summerized in the flow chart in Figure: 2.1. They are a set of Schrödinger like independent particle equations which must be solved subject to the condition that the effective potential ν_{eff} and the density $n(\mathbf{r})$ are consistent [63]. After solving Kohn-Sham equations, we will have a set of single electron wave functions. These wave functions can be used to calculate the new electron density. As an input, the new electron density is fed into the next cycle. Finally, after each iteration, compare the differences in calculated electron densities. If the difference in electron density between consecutive iterations is less than a suitably determined convergence threshold, the solution of the Kohn-Sham equations is deemed self-consistent. The predicted electron density has now been converted to the ground state electron density, which can be used to compute the total energy of the system [64].

2.9 The exchange-correlation (XC) functional

The exchange-correlation functional is at the core of density functional theory (DFT) that determines the accuracy of DFT in describing the interactions among electrons/ions in solids and molecules [65]. The crucial quantity in the Kohn-Sham approach is the exchange-correlation energy which is expressed as a functional of the density $E_{xc}[\mathbf{n}]$ [66]. The exchange-correlation potential for a homogeneous electron gas (HEG) at the electron density observed at position $\mathbf{r}$. This approximation uses only the local density to define the approximate exchange-correlation functional, hence called local density approximation (LDA) and widely used

$$
\begin{aligned}
E_{xc}^{LDA}(\mathbf{r}) &= \int n(\mathbf{r}\epsilon)_{xc}^{hom} n(\mathbf{r}) d\mathbf{r} \\
&= \int n(\mathbf{r}[\epsilon]_x^{hom} n(\mathbf{r}) + \epsilon)_c^{hom} n(\mathbf{r})] d\mathbf{r} \qquad (2.52) \\
&= E_{xc}^{LDA}[n(\mathbf{r})]
\end{aligned}
$$

The LDA is very simple, corrections to the exchange-correlation energy due to the inhomogeneities in the electronic density are ignored. Because of exchange-correlation

energy of inhomogeneous charge density can significantly different from HEG result. This leads to development of various generalized-gradient approximation (GGA). In the GGA approximation, the local electron density and local gradient in the electron density are included in the exchange and correlation energies [67]. One example of GGA functional used in DFT is the Perdew-Burke Ernzerhof (PBE) functional. It is formulated as

$$E_{xc}^{PBE} = E_{xc}^{LDA} + E_{c}^{PBE}. \tag{2.53}$$

Where, E_{xc}^{PBE} is the exchange correlation energy calculated using the PBE functional. E_{xc}^{LDA} is the exchange correlation energy calculated using LDA approximation and E_{c}^{PBE} is the correlation energy term specific to the PBE functional.

The exchange correlation potential was solved by GGA functional that understimates tha band gap value. Therefore, the modified Becke- Johnson exchange potential and LDA correlation by Trans and Blaha in 2009 (TB-mBJ) allows the calculation of band gaps with an accuracy similar to very expensive GW calculations.

<div style="text-align: right">

Chapter 3

</div>

Results and discussion

3.1   Computational methods

We have investigated the structural, electronic, optical and thermoelectric properties of NaGeBr$_3$ perovskite under various applied pressure. In this study, all the calculations have been carried out within WIEN2k code, which is an implementation of full potential linearized augmented plane wave (FP-LAPW) method in the density functional theory (DFT). The generalized gradient approximation (GGA) with the Perdew-Berke-Ernzerhof (PBE) for the evaluation of exchange correlation energy in Kohn-Sham equation. We used it for optimized ground states of NaGeBr$_3$. PBE-GGA functional understimates the electronic bandgap. Thus, local density approximation (LDA) with the modified Becke-Johnson (mBJ) potential of trans and Blaha was considered to obtain more accurate band gaps of electronic properties. Optical properties and thermoelectric properties has been carried out with the TB-mBJ potential. For optimizing the crystal structure, we set $R_{mt} \times K_{max} = 7.0$ where, R_{mt} is the smallest of the muffin-tin sphere radii and K_{max} is the largest reciprocal lattice vector used in the plane wave expansion. The number of k-points is selected to 1000 in Brillouin Zone, corresponding $10 \times 10 \times 10$ k-mesh, during calculation. We set the charge density is Fourier expanded up to $G_{max} = 12$ (Ry)$^{\frac{1}{2}}$. The

self-consistent calculations are considered converge when the convergence of energy
and convergence of charge are 0.00001 Ry and 0.001 e respectively.

3.2   Structural properties

The crystal structure of the cubic halide NaGeBr$_3$ perovskite resemble the ordered
cubic lattice structure with space group $Pm\bar{3}m$ (221). The lattice parameters are
equal in this crystal structure and the crystallographic angles are 90°. In the struc-
ture, the Na atom is located at 1a (0.0, 0.0, 0.0) Wyckoff position at the corner, the
Ge atom is placed at 1b (0.5, 0.5, 0.5) Wyckoff positions at the body center, and
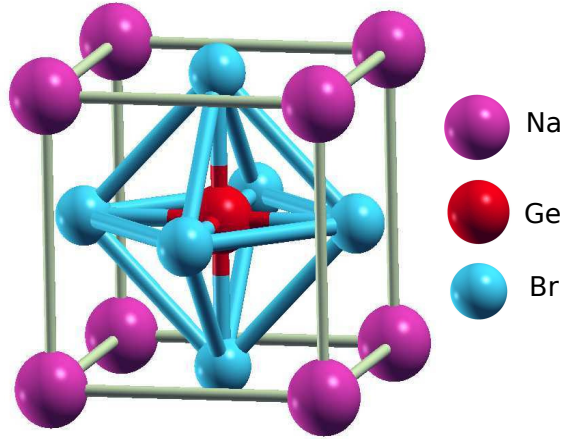the Br atoms is possess at 3c (0.5, 0.5, 0.5) Wyckoff position at the face center.

Figure 3.1: Crystal structure of cubic perovskite NaGeBr$_3$ at 0 GPa pressure.

We have performed this study under various hydrostatic pressure from 0 GPa to
4 GPa. At 0 GPa, the computed lattice constant of NaGeBr$_3$ is 5.52 Å, which is
relatively closure to the reference study 5.50 Å [68]. The daviation value of 0.37%
presents the high accuracy of this study.

The lattice constants are calculated by utilizing the PBE-GGA functional. The
optimized crystal structure and the variation of optimization energy with unit cell
volumes for NaGeBr$_3$ are represented in Figure: 3.1 and Figure: 3.2.

The application of hydrostatic pressure manifests a significant impact on lattice
constant. Table: 3.1 shows the calculated lattice constant and energy band gap of
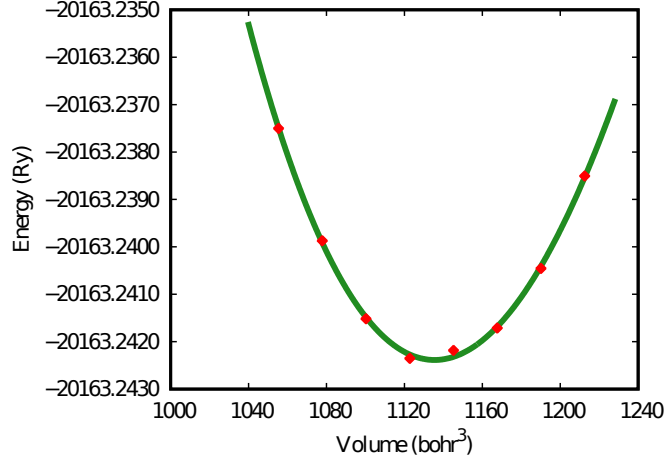
Figure 3.2: Energy versus unit cell volume curve of cubic perovskite NaGeBr$_3$ at 0 GPa pressure.

Table 3.1: Variation of lattice constants and band gap of NaGeBr$_3$ under pressure.

Pressures (GPa)	lattice constants (Å)	Band gap (eV)
0	5.52	0.81
1	5.45	0.57
2	5.38	0.35
3	5.32	0.12
4	5.27	0.00

NaGeBr$_3$ at various applied pressure. The calculated lattice constant decreases at a different rates over different pressure.

3.3   Electronic properties

The study of electronic properties is crucial to gain a clear concept about optical properties of NaGeBr$_3$ halide perovskite. The basic electronic properties including band structure and density of states (DOS). Partial density of states is important to know the different angular momentum component contribution. It provides information to identify the nature of orbitals whether the states are s-like or p-like. The charge density helps to understand the chemical bonding in NaGeBr 3 and maintain their ionic and covalent bonds, Na-Br and Ge-Br, respectively. The electronic band structure, density of states and charge density under various pressure are calculated

and discussed in this section.

3.3.1 Band structure

The electronic band structure is necessary to understand the phyical properties of crystalline solids which describe optical as well as transport properties. The band structures of NaGeBr$_3$ perovskite at different applied pressure are shown in Figure: 3.3. The horizontal dotted line at 0 eV denotes the Fermi level (E_F), whereas the valence band (VB) and conduction band (CB) are presented by colored line below and above the E_F respectively.
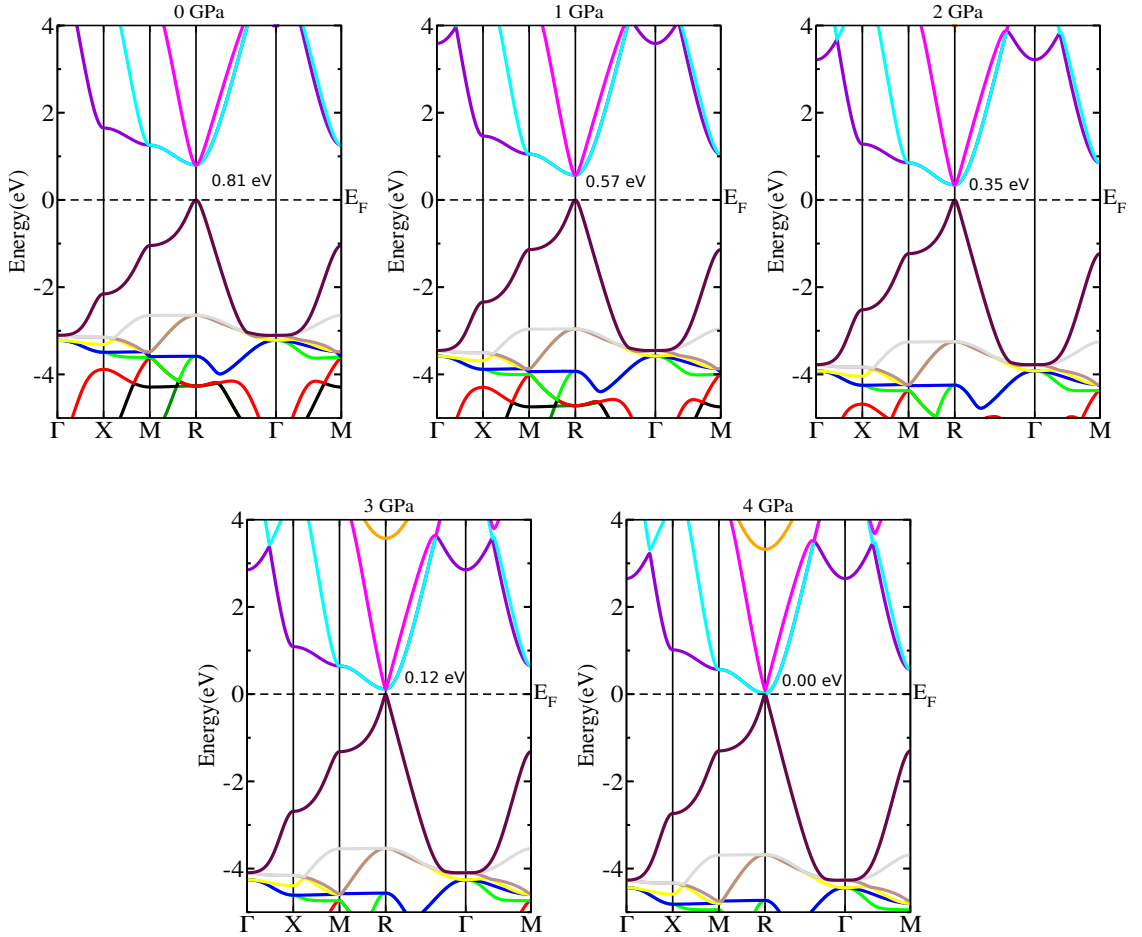

Figure 3.3: The band structure of NaGeBr$_3$ under various pressures.

The calculation is done by defining highly symmetric points on the edge of the Brillouin Zone (BZ) with sampling path of Γ-X-M-R-Γ-M. This study illustrates the

band structure around the E_F ranging from -5 eV to $+4$ eV. The conduction bands minima (CBM) and the valence band maxima (VBM) for $NaGeBr_3$ perovskite are located at the R point of the BZ. Therefore a direct band gap (E_g) is found for $NaGeBr_3$ perovskite. The observed energy band gap is 0.55 eV as calculated by the PBE-GGA functional and 0.81 eV as calculated by TB-mBJ functional. The PBE-GGA functional understimates the electronic bandgap, where the TB-mBJ functional gives band gap values close to the experimental ones. We shows from the Figure: 3.3 that the elevated pressure from 0 to 4 GPa leads to the gradual decrease in band gaps as 0.81 eV to 0.00 eV for $NaGeBr_3$ perovskite. As a result, the valence band and the conduction band overlap and enhance the optical conductivity of metal halide.

3.3.2 Density of states

The electronic states of a solid are described by a quantity called density of states (DOS). In order to describe the electronic band structure, we looked at DOS. We have investigated the changes in the DOS of the $NaGeBr_3$ perovskite under hydrostatic pressures from 0 to 4 GPa. Figure: 3.4 shows the computed total and partial density of states of $NaGeBr_3$ perovskite at ambient and applied pressures.

For getting a material's atomic contribution for creating it's band structure, PDOS is essential. From the Figure: 3.4, The black vertical dased line at 0 eV represents the fermi level energy, E_F. For the valence band, it can be noticed that the DOS is largely contributed by the Br-4p orbital with a small participation of Ge-4p and Na-3s orbital under hydrostatic pressure. For the conduction band, the DOS is largely originates from Ge-4p orbitals with small participation of Br-4p. The TDOS of $NaGeBr_3$ perovskite under pressure for a deeper understanding. The DOS at the fermi level for $NaGeBr_3$ perovskite is seen to be zero at 4 GPa pressure that causes semiconductor to metallic electrical phase transition.
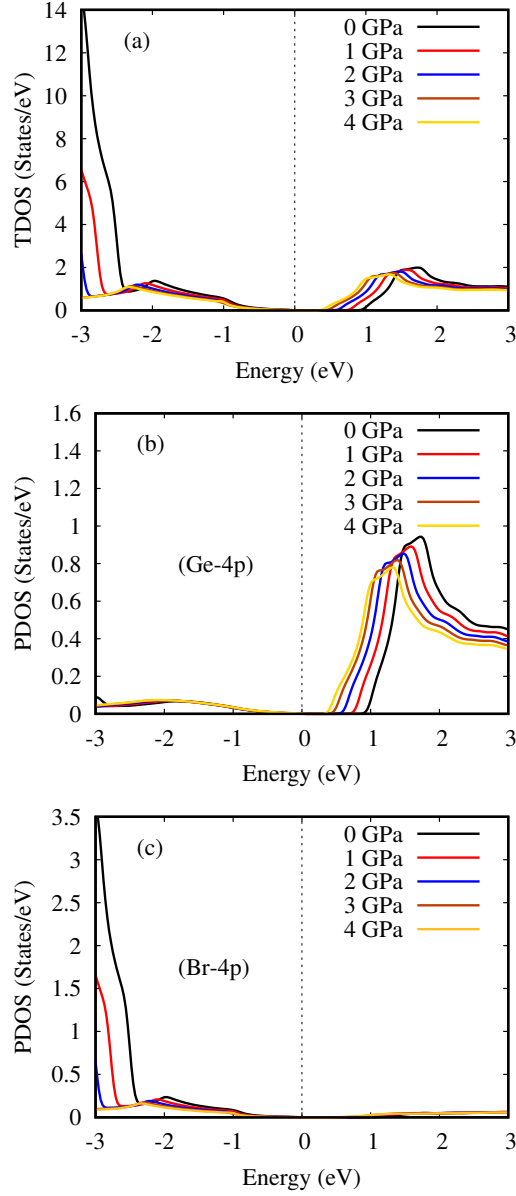
Figure 3.4: The total (TDOS) and the partial density of states (PDOS) of NaGeBr$_3$ cubic halide perovskite under pressures.

3.3.3 The charge density

The charge density is the measurement of electric charge per unit area of a surface. It indicates how much charge is stored in a particular field. In Figure: 3.5 and Figure: 3.6, using the charge density mapping along the crystallographic planes (100) and (101) planes at 0 GPa to 4 GPa pressures help to understand the chemical bonding in NaGeBr$_3$ perovskite.

Ionic bonding between Na and Br atoms is demonstrated by the charge distribution
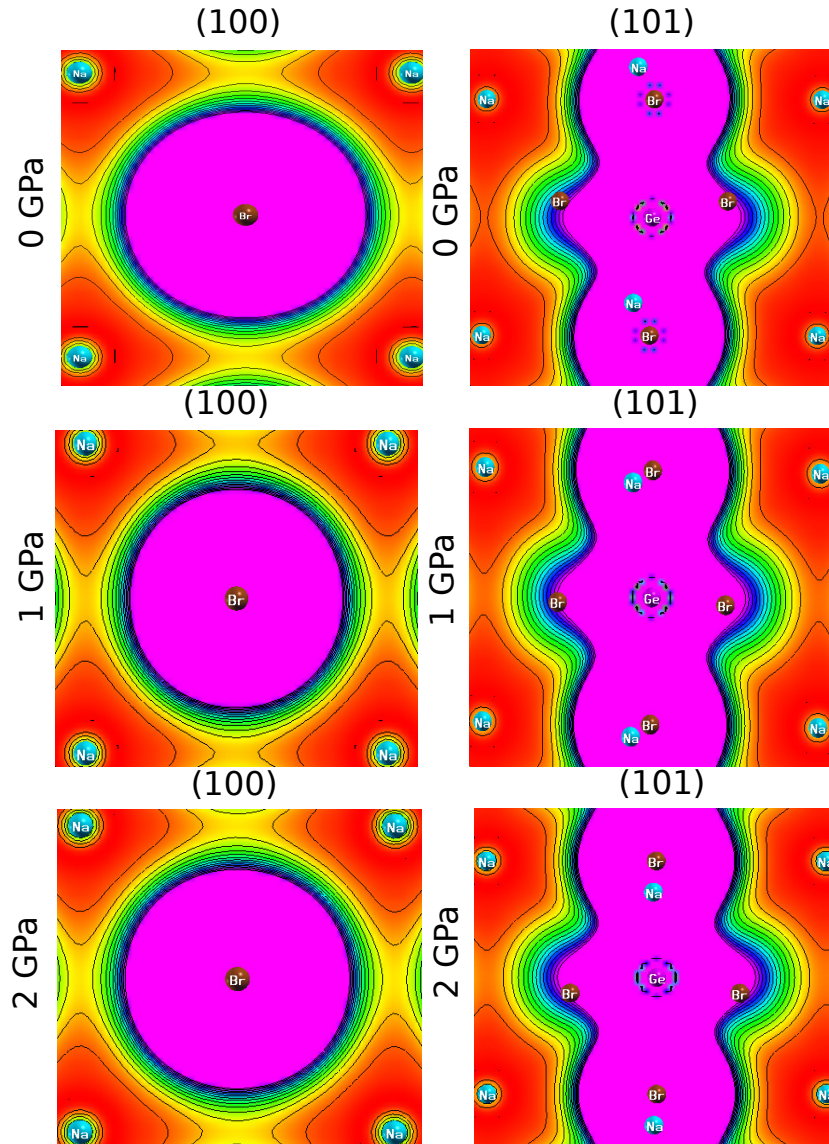
Figure 3.5: The charge density plots of NaGeBr$_3$ along (100) and (101) plane under various pressures.

of these two atoms because they donot overlapping along the (100) plane at 0 GPa. But there is a tiny overlap between Ge and Br atoms along the (101) plane, indicating the covalent bond. The ionic nature of Na-Br interactions are remain unchanged as pressure increased. The covalent nature of Ge-Br interactions is strengthned because overlapping of Ge and Br atoms increased along (101) plane.
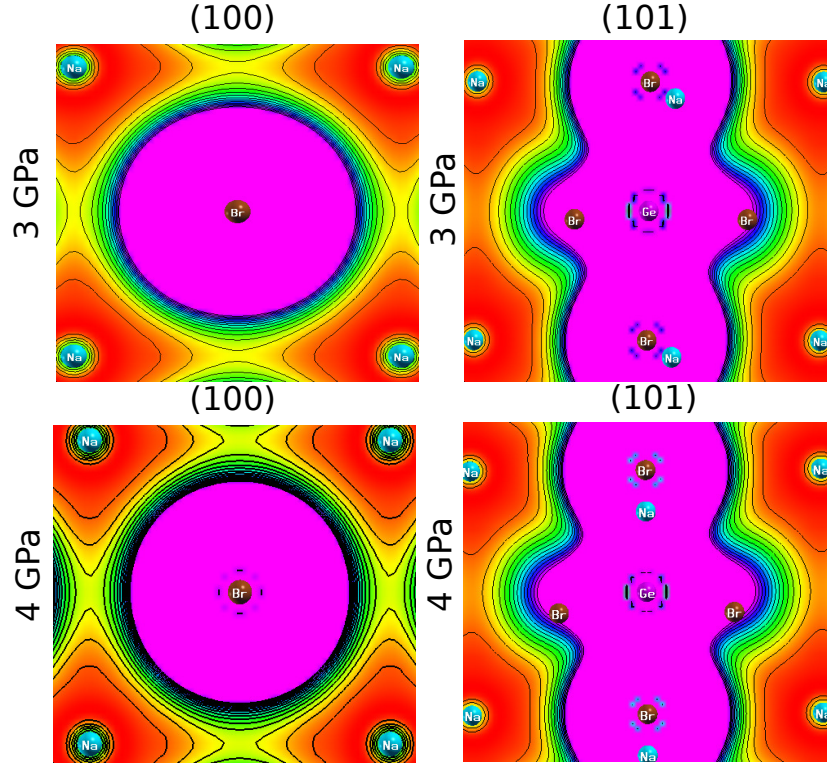
Figure 3.6: The charge density plots of NaGeBr$_3$ along (100) and (101) plane under various pressures.

3.4   Optical properties

We have calculated optical properties of NaGeBr$_3$ halide perovskites. NaGeBr$_3$ possess high reflectivity, less optical conductivity and moderate absorption nature. Thus it is not better option for perovskite solar cell. Therefore, to make it better efficiency perovskite solar cell, pressure can be applied. Optical properties includes real and imaginary part of dielectric constant, absorption coefficient, reflectivity, optical conductivity, extinction coefficient, refractive index and electron energy loss of NaGeBr$_3$ are analyzed and discuss under hydrostatic pressure from 0 GPa to 4 GPa.

3.4.1   Dielectric function

Dielectric resembles the relationship between energy band structure and optical transition. To figure out the amount of electromagnetic radiation response in sample, we must utilize the complex dielectric function.
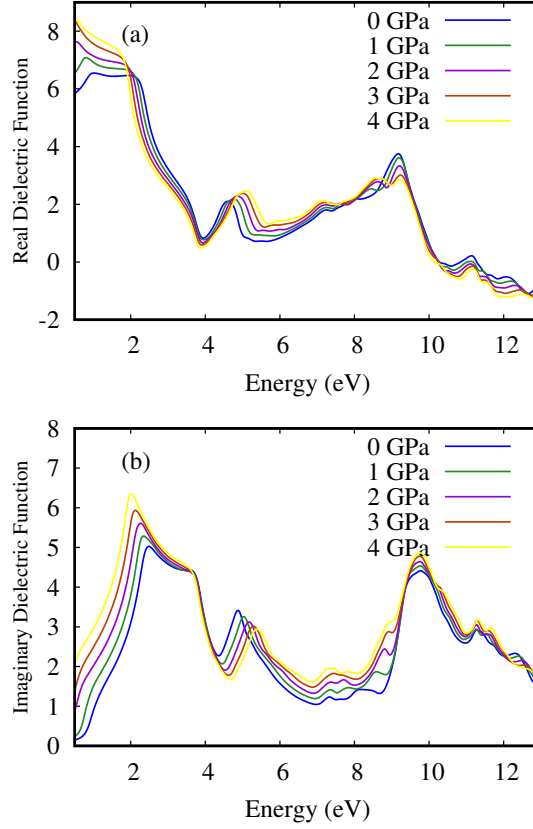
Results and discussion

Figure 3.7: (a) Real part of dielectric function $\epsilon_1(\omega)$ and (b) imaginary part of dielectric function $\epsilon_2(\omega)$

.

The complex dielectric function written as

$$\varepsilon(\omega) = \varepsilon_1(\omega) + i\varepsilon_2(\omega). \tag{3.1}$$

Where, $\varepsilon_1(\omega)$ and $\varepsilon_2(\omega)$ are represents real and imaginary parts of the dielectric function. The electronic polarization of the compound is explains in real part and electron excitation is explains in an imaginary part of complex dielectric function. In Figure: 3.7, we showed the real and imaginary dielectric function versus energy for $NaGeBr_3$ under various applied pressure upto 0 GPa to 4 GPa obtained from mBJ potential. At hydrostatic pressure, $NaGeBr_3$ displays the peaks are shifted towards higher energy values that means the value of $\varepsilon_1(\omega)$ increases with induced pressure and decreases with photon energy. Which indicates, $\varepsilon_1(\omega)$ rises in the infrared-visible region and falls in the ultraviolet region. In Figure: 3.7 the visible and UV region has a greater $\varepsilon_2(\omega)$ at 0 GPa which indicates a high absorption level

27

but spectrum shifts to the low energy region under high pressure.

3.4.2   Optical reflectivity

Optical reflectivity is a determination of a surface's capacity of reflect light. In Figure: 3.8 (a), we showed the reflectivity versus energy of NaGeBr$_3$ to used to understand the surface nature. When applied various hydrostatic pressure from 0 GPa to 4 GPa, the reflectivity of NaGeBr$_3$ has rises, these transits from the infrared to visible region. Afer transiting to the ultraviolet region, these exhibits highest peaks. That's why it reduces the strength of the solar cell under various pressure. Thus, NaGeBr$_3$ may be employed as a coating to reduce solar heating.
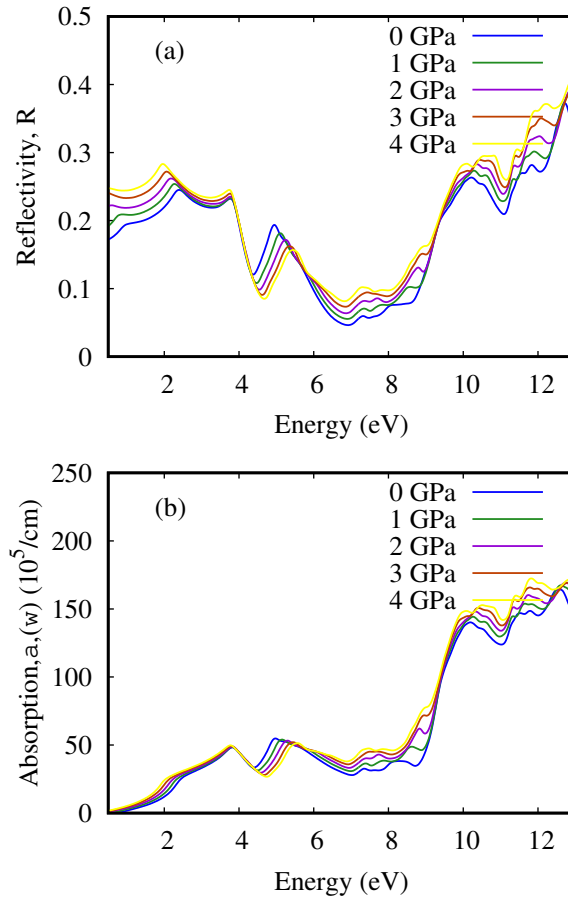

Figure 3.8: (a) Optical reflectivity and (b) Absorption coefficient as a function of energy for NaGeBr$_3$ under various pressure.

3.4.3 Absorption coefficient

The fraction of energy (wavelength) absorbed per unit length of the material is known as optical absorption coefficient. It provides the information about the efficiency of solar energy conversion of a material. Figure: 3.8 (b) shows the absorption coefficient versus energy of NaGeBr$_3$ for 0 GPa to 4 GPa. The absorption coefficient at different pressures in the range of 0 eV to 13 eV. The Figure displays that the absorption coefficient is increased under applied hydrostatic pressure, which indicates the better efficiency of the NaGeBr$_3$ perovskite solar cell.

3.4.4 Refractive index

The refractive index is an important parameter to measure, how much light bends or reflects through the optical medium.
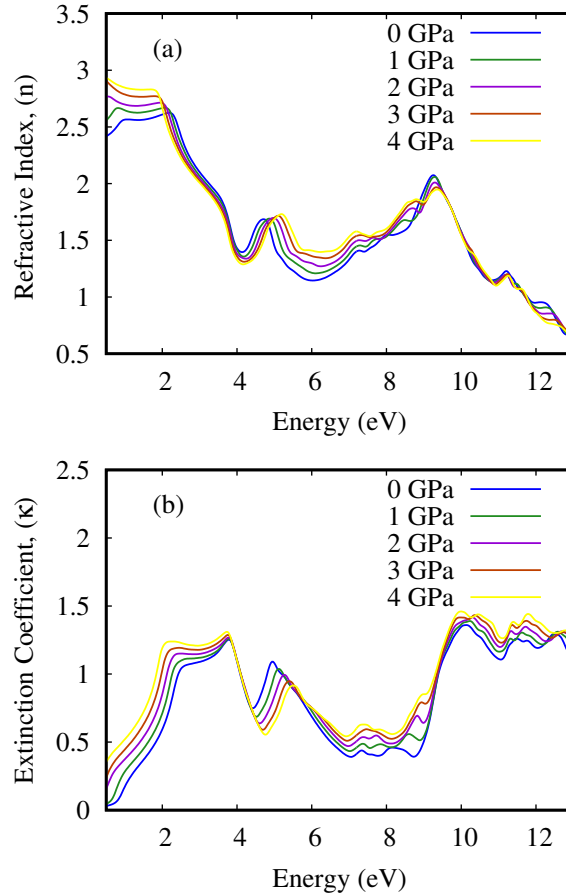

Figure 3.9: (a) Refractive Index and (b) Extinction coefficient as a function of energy for NaGeBr$_3$ under various pressure.

The refractive index and the band gap are inversly related as the refractive index rises, the bandgap falls and vice-versa. In Figure: 3.9 (a), We have plotted refractive index versus energy for $NaGeBr_3$ under various pressure. From the figure we showed that refractive index decreases steadily from the infrared to ultraviolet region.

3.4.5 Extinction coefficient

The strength how effectively an element absorbs or reflects radiation or light at certain wavelengths is determined by it's extinction coefficient.The Figure: 3.9 (b) showed the extinction coefficient for $NaGeBr_3$ halide perovskite under applied hydrostatic pressure upto 0 GPa to 4 GPa. The extinction coefficient is increased with increasing pressure and peaks are shifted to the UV region with increasing photon energy.

3.4.6 Optical conductivity

A characteristics of a material that indicates the relationship between the inducing electric fields magnitudes and the materials induced current density is known as optical conductivity. It provides information about materials atomic level electronic structure and behaviour. Figure: 3.10 (a) illustrates the optical conductivity versus energy of $NaGeBr_3$ at 0 GPa to 4 GPa pressures. With increasing energy, $NaGeBr_3$ exhibits optical conductivity at ultraviolet region under applied pressure.

3.4.7 Electron energy loss

The energy lost by a fast moving electron as it travel through a material is known as electron energElectron energy loss function versus energy is shown in Figure: 3.10 (b) for $NaGeBr_3$ under various pressure. We showed that in infrared-visible region, electron energy loss is increased with increasing pressure. After transition of UV region, the electron energy loss is decreased with increasing pressure.
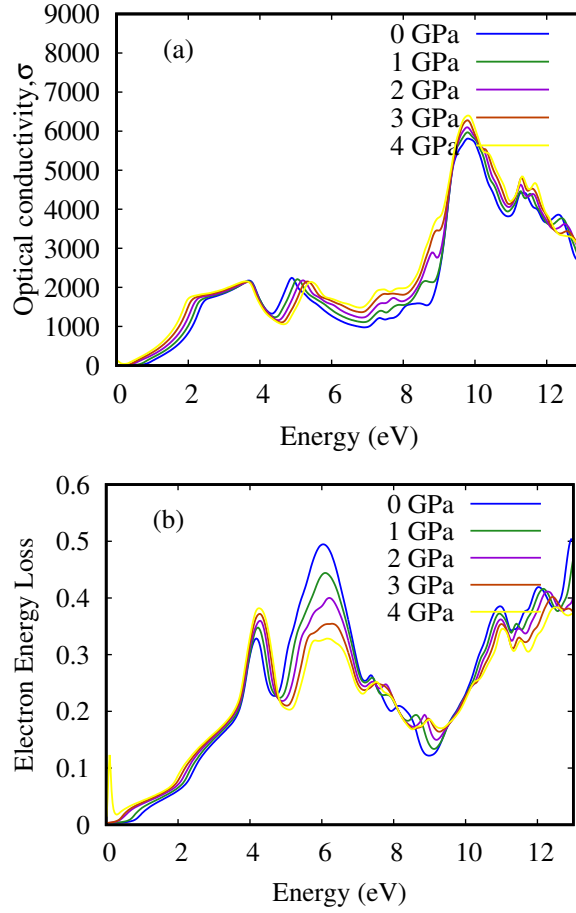
Figure 3.10: (a) Optical conductivity and (b) Electron energy loss as a function of energy for NaGeBr$_3$ under various pressure.

3.5 Thermo-electric properties

Thermal energy can be converted into electrical energy in thermoelectric material by using the potential difference produced by the heat gradient during energy transmission. The thermoelectric properties have been calculated for NaGeBr$_3$ halide perovskite under hydrostatic pressure using Boltztrap package. We determined the transport coefficients such as the Seebeck coefficient (S), electrical conductivity σ/τ, thermal conductivity (κ), power factor ($S^2\sigma$) and dimensionless figure of merit (ZT) as a function of temperature combined in a compressed form as

$$ZT = \frac{S^2\sigma T}{\kappa}. \tag{3.2}$$

The Seebeck coefficient of a material is a measure of the magnitude of an induced

Results and discussion
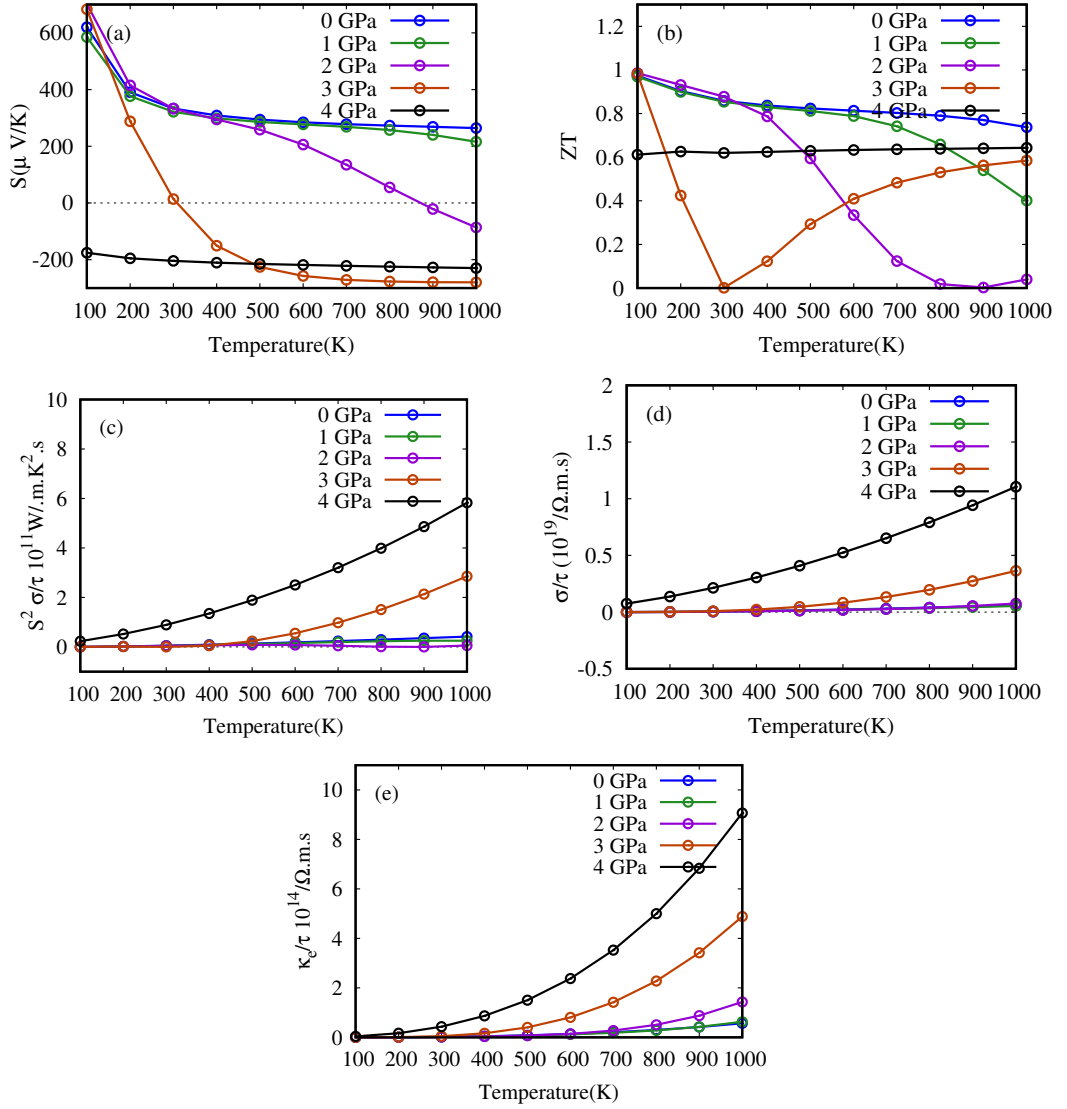
Figure 3.11: Thermoelectric properties as (a) Seebeck coefficient, (b) Figure of merit (ZT), (c) Power factor, (d) Electrical conductivity and (e) Thermal conductivity of NaGeBr$_3$ under various pressures.

thermoelectric voltage in response to a temperature difference across that material, which can be seen in mathematical form $S = \mu \nabla V / \nabla T$. In Figure: 3.11 (a), We investigated the Seebeck coefficient against temperature for NaGeBr$_3$ under different pressures upto 4 GPa. Seebeck coefficient decreased with rising temperature and also decreased under pressure. The figure of merit (ZT) is used to measure the materials quality for thermal devices. The figure of merit (ZT) values of NaGeBr$_3$ has been examined as shown in Figure: 3.11 (b). Power factor of a material provides electrical energy. The power factor of NaGeBr$_3$ displays in Figure: 3.11 (c) that rising with applied pressure against temperature (T). Electrical conductivity

defines the concentration of free electron. Figure: 3.11 (d) showed that electrical conductivity increased under applied pressure and also increased with temperature. Finally, Thermal conductivity describes the transportation through a material as the materials atom are constantly moving in rotational, translational or vibrational motion. The variation of atoms is responsible for generating heat or thermal energy in a material. Figure: 3.11 (e) showed the thermal conductivity of $NaGeBr_3$ under various pressure. From the figure thermal conductivity increased with increasing pressure against temperature (T).

<div align="right">

Chapter 4

</div>

Conclusion

The study systematically explored the structural, electronic, optical, and thermoelectric properties of cubic NaGeBr$_3$ perovskite using the WIEN2k code within the framework of the DFT-based FP-LAPW method under hydrostatic pressures ranging from 0 GPa to 4 GPa. At ambient pressure, the lattice parameter of NaGeBr$_3$ perovskite is found to be 5.52 Å, diminishing with increasing pressure. The calculated direct energy band gap is 0.81 eV using the TB-mBJ functional. As pressure rises, the band gap reduces, signifying a transition from a semiconducting to a metallic state at 4 GPa pressure. Analysis of the density of states (DOS) reveals the dominance of p-states of Br atoms near the top of the valence band, while the Ge-p orbital contributes significantly near the bottom of the conduction band. The charge density provides insights into the ionic and covalent bonds, namely Na-Br and Ge-Br. The study also covers the absorption coefficient calculation, dielectric functions, optical conductivity, and other optical properties of NaGeBr$_3$ under hydrostatic pressures. Thermoelectric properties, computed using the BoltzTraP code, indicate an increase in electrical conductivity, thermal conductivity, and power factor, accompanied by a decrease in the Seebeck coefficient with rising pressure. The findings suggest the potential suitability of pressure-induced NaGeBr$_3$ material for optoelectronic devices, particularly in solar cells and photovoltaic applications.

Bibliography

[1] Robert C. Liebermann. Elasticity of the ilmenite - perovskite phase transformation in CdTiO$_3$. *Phys. Earth Planet. Inter.*, 29:326–332, 1976.

[2] Arthur J Freeman. Antagonism between spin-orbit coupling and steric effects causes anomalous band gap evolution in the perovskite photovoltaic materials CH$_3$NH$_3$Sn$_1$-xPbxI$_3$. *J Phys Chem Lett*, 2015.

[3] Radi A. Jishi, Oliver B. Ta, and Adel A. Sharif. Modeling of lead halide perovskites for photovoltaic applications. *J. Phys. Chem. C*, pages 28344–28349, 2014.

[4] Juan Bisquert. The physics of solar cells: Perovskites, organics, and photovoltaic fundamentals. *Cryst. Growth Des.*, 2017.

[5] Constantinos C. Stoumpos, Christos D. Malliakas, John A. Peters, Zhifu Liu, Maria Sebastian, Jino Im, Thomas C. Chasapis, Arief C. Wibowo, Duck Young Chung, Arthur J. Freeman, Bruce W. Wessels, and Mercouri G. Kanatzidis. Crystal growth of the perovskite semiconductor CsPbBr$_3$: A new material for high-energy radiation detection. *Cryst. Growth Des.*, 13:2722–2727, 2013.

[6] Fried T. Poddar P. et al Markovich, G. Observation of the verwey transition in Fe$_3$O$_4$ nanocrystals. *MRS Online Proceedings Library*.

[7] B. Bouadjemi, S. Bentata, A. Abbad, W. Benstaali, and B. Bouhafs. Half-metallic ferromagnetism in PrMnO$_3$ perovskite: First principles calculations. *Solid State Commun.*, 168:06–10, 2013.

[8] Shakeel Ahmad Khandy, Ishtihadah Islam, Dinesh C Gupta, Rabah Khenata, A Laref, and Seemin Rubab. DFT understandings of structural properties, me-

chanical stability and thermodynamic properties of $BaCfO_3$ perovskite. *Mater. Res. Express*, 5:105702, 2018.

[9] R. Terki, Houda Imane Faraoun, Ghislaine Bertrand, and Hafid Aourag. Full potential calculation of structural, elastic and electronic properties of $BaZrO_3$ and $SrZrO_3$. *Phys. Status Solidi (b)*, 242:1024–1062, 2005.

[10] J. B. Torrance, P. Lacorre, A. I. Nazzal, E. J. Ansaldo, and Niedermayer. Systematic study of insulator-metal transitions in perovskites $RNiO_3$ (R=Pr,Nd,Sm,Eu) due to closing of charge-transfer gap. *Phys. Rev. B*, 45, 1992.

[11] Jeffrey W. Fergus. Perovskite oxides for semiconductor-based gas sensors. *Sens. Actuators B Chem.*, 123:1169–1179, 2007.

[12] Martin Green, Anita Ho-Baillie, and Henry Snaith. The emergence of perovskite solar cells. *Nat. Photonics*, 8, 2014.

[13] Stoumpos C. Cao D. Hao, F. Lead-free solid-state organic–inorganic halide perovskite solar cells. *Nat. Photonics*, 2014.

[14] H.J Snaith. Perovskites: The emergence of a new era for low-cost, high-efficiency solar cells. *J. Phys. Chem. Lett.*, 2013.

[15] He T, Ramirez AP Huang Q, Regan KA Wang Y, Hayward MA Rogado N, Slusky JS Haas MK, Zandbergen HW Inumara K, and Cava RJ Ong NP. Superconductivity in the non-oxide perovskite $MgCNi_3$. *Nature.*, 2001.

[16] Cohen RE. Fu H. Polarization rotation mechanism for ultrahigh electromechanical response in single-crystal piezoelectrics. *Nature.*, 2000.

[17] Y. Yamasaki, H. Sagayama, N. Abe, T. Arima, K. Sasai, M. Matsuura, K. Hirota, D. Okuyama, Y. Noda, and Y. Tokura. Cycloidal spin order in the *a*-axis polarized ferroelectric phase of orthorhombic perovskite manganite. *Phys. Rev. Lett.*, 2008.

[18] Moghaddam R. Lai M. Tan, ZK. Bright light-emitting diodes based on organometal halide perovskite. *Nat. Nanotechnol.*, 2014.

[19] Hayatullah, S. Naeem, G. Murtaza, R. Khenata, and M.N. Khalid. First principle study of $CsSrM_3$ (M=F, Cl). *Phys. B Con-dens. Matter*, 414:91–96, 2013.

Bibliography

[20] Quinten A. Akkerman, Marina Gandini, Francesco di Stasio, Prachi Rastogi, Francisco Palazon, Giovanni Bertoni, James M. Ball, Mirko Prato, Annamaria Petrozza, and Liberato Manna. Strongly emissive perovskite nanocrystal inks for high-voltage solar cells. *Nat. Energy*, 2:16194, 2016.

[21] Giles E. Eperon, Giuseppe M. Paternò, Rebecca J. Sutton, Andrea Zampetti, Amir Abbas Haghighirad, Franco Cacialli, and Henry J. Snaith. Inorganic Caesium Lead Iodide perovskite solar cells. *J. Mater. Chem. A*, 3:19688–19695, 2015.

[22] Thirumal Krishnamoorthy, Hong Ding, Chen Yan, Wei Lin Leong, Tom Baikie, Ziyi Zhang, Matthew Sherburne, Shuzhou Li, Mark Asta, Nripan Mathews, and Subodh G. Mhaisalkar. Lead-free germanium iodide perovskite materials for photovoltaic applications. *J. Mater. Chem. A*, 3:23829–23832, 2015.

[23] Parthiban Ramasamy, Da-Hye Lim, Bumjin Kim, Seung-Ho Lee, Min-Sang Lee, and Jong-Soo Lee. All-inorganic cesium lead halide perovskite nanocrystals for photodetector applications. *Chem. Commun.*, 52:2067–2070, 2016.

[24] Ajay Kumar Jena, Ashish Kulkarni, and Tsutomu Miyasaka. Halide perovskite photovoltaics: Background, status, and future prospects. *Chem. Rev.*, 119:3036–3103, 2019.

[25] Xin-Gang Zhao, Gustavo M. Dalpian, Zhi Wang, and Alex Zunger. Polymorphous nature of cubic halide perovskites. *Phys. Rev. B*, 15:155137, 2020.

[26] A. Oleaga, A. Salazar, and D. Skrzypek. Critical behaviour of magnetic transitions in $KCoF_3$ and $KNiF_3$ perovskites. *J. Alloys Compd*, 629:178–183, 2015.

[27] Aslihan Babayigit, Dinh Duy Thanh, Anitha Ethirajan, Jean Manca, Marc Muller, Hans-Gerd Boyen, and Bert Conings. Assessing the toxicity of Pb- and Sn-based perovskite solar cells in model organism danio rerio. *Sci. Rep.*, 6:18721, 2016.

[28] BJ, DeQuilettes DW van Franeker JJ, Sutton RJ Pathak S, Ginger DS Grancini G, Petrozza A Janssen RA, and Snaith HJ. The importance of moisture in hybrid lead halide perovskite thin film fabrication. *PMID: 26247197*, 2015.

[29] Ethirajan A. Muller M Babayigit, A. Toxicity of organometal halide perovskite solar cells. *Nat. Mater.*, 2016.

Bibliography

[30] Mohammad Abdur Rashid, Md Saiduzzaman, Arpon Biswas, and Khandaker Hossain. First-principles calculations to explore the metallic behavior of semiconducting lead-free halide perovskites $RbSnX_3$ (X = Cl, Br) under pressure. *Eur. Phys. J. Plus*, 13:649, 2022.

[31] Bo Wu, Weihua Ning, Qiang Xu, Manukumara Manjappa, Minjun Feng, Senyun Ye, Jianhui Fu, Stener Lie, Tingting Yin, Feng Wang, Teck Wee Goh, Padinhare Cholakkal Harikesh, Yong Kang Eugene Tay, Ze Xiang Shen, Fuqiang Huang, Ranjan Singh, Guofu Zhou, Feng Gao, and Tze Chien Sum. Strong self-trapping by deformation potential limits photovoltaic performance in Bismuth double perovskite. *Sci.Adv.*, 2021.

[32] Zhenyun Lan, Jie Meng, Kaibo Zheng, and Ivano Castelli. Exploring the intrinsic point defects in Cesium Copper halides. *J. Phys. Chem. C*, 125, 2021.

[33] Dhanashree Moghe, Lili Wang, Christopher J. Traverse, Adam Redoute, Melany Sponseller, Patrick R. Brown, Vladimir Bulović, and Richard R. Lunt. All vapor-deposited lead-free doped $CsSnBr_3$ planar solar cells. *Nano Energy*, 28:469–474, 2016.

[34] Mohammed Houari, B. Bouadjemi, Slimane Haid, Matougui Mohamed, Tayeb Lantri, Zoubir Aziz, Samir Bentata, and B. Bouhafs. Semiconductor behavior of halide perovskites $AGeX_3$ (A = K, Rb and Cs; X = F, Cl and Br): First-principles calculations. *Indian J. Phys.*, 94, 2019.

[35] Chaiyawat Kaewmeechai, Yongyut Laosiritaworn, and Atchara Punya Jaroenjittichai. Electronic structure of nontoxic-inorganic perovskite: $CsMgBr_3$ using DFT calculation. *J. Phys. Conf. Ser.*, 2019.

[36] Safin Alam, Md Saiduzzaman, Arpon Biswas, Tanjun Ahmed, Aldina Sultana, and Khandaker Hossain. Tuning band gap and enhancing optical functions of $AGeF_3$ (A = K, Rb) under pressure for improved optoelectronic applications. *Sci. Rep.*, 12:8663, 2022.

[37] Constantinos C. Stoumpos, Laszlo Frazer, Daniel J. Clark, Yong Soo Kim, Sonny H. Rhim, Arthur J. Freeman, John B. Ketterson, Joon I. Jang, and Mercouri G. Kanatzidis. Hybrid Germanium Iodide perovskite semiconductors: Active lone pairs, structural distortions, direct and indirect energy gaps, and strong nonlinear optical properties. *J. Am. Chem. Soc.*, 137:6804–6819, 2015.

Bibliography

[38] Imane Hamideddine, Hassan Zitouni, Najim Tahiri, El Bounagui Omar, and Hamid Ez-Zahraouy. A DFT study of the electronic structure, optical, and thermoelectric properties of halide perovskite $KGeI_3$-XBrX materials: photovoltaic applications. *Appl. Phys. A*, 127, 2021.

[39] Jakiul Islam and A.K.M. Hossain. Semiconducting to metallic transition with outstanding optoelectronic properties of $CsSnCl_3$ perovskite under pressure. *Sci. Rep.*, 10, 2020.

[40] Md Kholil and Md. Tofajjol Bhuiyan. Effects of pressure on narrowing the band gap, visible light absorption, and semi-metallic transition of lead-free perovskite $CsSnBr_3$ for optoelectronic applications. *J. Phys. Chem. Solids*, 2021.

[41] M. A. Islam, Md. Zahidur Rahaman, and Sapan Kumar Sen. A comparative study of hydrostatic pressure treated environmentally friendly perovskites $CsXBr_3$ (X = Ge/Sn) for optoelectronic applications. *AIP Adv.*, 11:075109, 2021.

[42] Md. Sajib Hossain, Md. Majibul Haque Babu, Tusar Saha, Md. Sazzad Hossain, Jiban Podder, Md. Shohel Rana, Abdul Barik, and Protima Rani. Pressure induced semiconductor to metal phase transition in cubic $CsSnBr_3$ perovskite. *AIP Adv.*, 11:055024, 2021.

[43] T Britannica. Editors of encyclopaedia. *encyclopedia britannica*, 2020.

[44] Franz Schwabl. Quantenmechanik. *Springer Sci. Rev.*, 7, 2008.

[45] David J Griffiths. An introduction to quantum mechanics, volume 2 nd. *pearson education*, 2005.

[46] Arthur Jabs. Connecting spin and statistics in quantum mechanics. *Found. Phys.*, 40:776–792, 2010.

[47] Wolfgang Pauli. On the connexion between the completion of electron groups in an atom with the complex structure of spectra. *Zeitschrift für Physik*, 31:765, 1925.

[48] Nouredine Zettili. Quantum mechanics: concepts and applications. *AAPT*, 2003.

[49] Jean-Michel Combes, Pierre Duclos, and Ruedi Seiler. The Born-Oppenheimer approximation. *Springer*, pages 185–213, 1981.

Bibliography

[50] Hanno Essén. The physics of the Born-Oppenheimer approximation. *Int. J. Quantum Chem*, 12:721–735, 1977.

[51] Wolfram Koch and MC Holthausen. A chemist's guide to density functional theory, 2001. *Wiley-VCH Verlag GmbH*, 1989.

[52] Asger Halkier, Trygve Helgaker, Poul Jørgensen, Wim Klopper, and Jeppe Olsen. Basis-set convergence of the energy in molecular Hartree–Fock calculations. *Chem. Phys. Lett.*, 302:437–446, 1999.

[53] Philippe C Hiberty, Stephane Humbel, David Danovich, and Sason Shaik. What is physically wrong with the description of odd-electron bonding by Hartree-Fock theory? a simple nonempirical remedy. *J. Am. Chem. Soc.*, 117:9003–9011, 1995.

[54] Ida Josefsson, Kristjan Kunnus, Simon Schreck, Alexander Fohlisch, Frank de Groot, Philippe Wernet, and Michael Odelius. Ab initio calculations of x-ray spectra: Atomic multiplet and molecular orbital effects in a multiconfigurational scf approach to the l-edge spectra of transition metal complexes. *. Phys. Chem. Lett.*, 3:3565–3570, 2012.

[55] Pierre Hohenberg and Walter Kohn. Inhomogeneous electron gas. *Phys. Rev.*, 136:B864, 1964.

[56] Walter Kohn. Nobel lecture: Electronic structure of matter—wave functions and density functionals. *RMP*, 71:1253, 1999.

[57] WD Myers and WJ Swiatecki. Nuclear properties according to the Thomas-Fermi model. *Nucl. Phys.*, 601:141–167, 1996.

[58] WD Myers and WJ Swiatecki. A Thomas-Fermi model of nuclei. part i. formulation and first results. *Ann. Phys.*, 204:401–431, 1990.

[59] John Ferreirinho, Remo Ruffini, and Luigi Stella. On the relativistic Thomas-Fermi model. *Phys. Lett. B*, 91:314–316, 1980.

[60] JA Camargo-Martínez and R Baquero. Performance of the modified Becke-Johnson potential for semiconductors. *Phy.Rev.B*, 86:195106, 2012.

Bibliography

[61] Diola Bagayoko, Yacouba Issa Diakité, and Lashounda Franklin. Comments on all-electron self-consistent gw in the matsubara-time domain: Implementation and benchmarks of semiconductors and insulators. *arXiv preprint arXiv:1610.04657*, 2016.

[62] Robert G. Parr and Weitao Yang. The Kohn-Sham method: basic principles. *Oxford University Press, Inc.*, 1989.

[63] I Richard M. Martin. Electronic structure: basic theory and practical methods. *Cambridge University Press*, pages 172–174, 2004.

[64] R. Bauernschmitt and Ahlrichs. Stability analysis for solutions of the closed shell Kohn-Sham equation. *J. Chem. Phys.*, 104(22):9047–9052, 1996.

[65] Xiaofei Shao, Peitao Liu, Cesare Franchini, Yi Xia, and Jiangang He. Assessing the performance of exchange-correlation functionals on lattice constants of binary solids at room temperature within the quasiharmonic approximation. *Phys. Rev. B*, 108:024306, 2023.

[66] Richard M. Martin. Electronic structure: basic theory and practical methods. *http://www.cambridge.org*, page 152, 2004.

[67] J.A. Steckel D.S. Sholl. Density functional theory: a practical introduction. *John Wiley Sons*, 2009.

[68] Larbi Setti Redi Kristian Pingak, Soukaina Bouhmaidi. Investigation of structural, electronic, elastic and optical properties of Ge-halide perovskites $NaGeX_3$ (X = Cl, Br and I): A first-principles DFT study. *Phys. B: Condens.*, 663:415003, 2023.